VELOCITY MEASUREMENTS IN WAVE BOUNDARY LAYER FLOW OVER A RIPPLED BED

by

Janaka J Wijetunge

Abstract

Velocity measurements in wave boundary layer flow over a rippled bed are presented. The fluid velocities, both the horizontal and the vertical components, were measured with a laser Doppler anemometer. The velocity records close to the rippled bed clearly show the perturbations caused by the vortices that form on the lee-side of the ripples. Consequently, plots of vorticity contours have been used to examine closely the formation, growth, and subsequent ejection and decay of lee-vortices. Further, the Eulerian drift velocities computed from the measured velocity records indicate the presence of a pair of re-circulating cells per ripple wave length. It also appears that peak drift velocities initially rise steeply with the ratio between the orbital amplitude and the ripple wave length, reach a maximum and then fall again. Finally, the spatially averaged peak turbulence over ripples is compared with that above three dimensional rough beds. The comparison shows that the turbulence intensities over ripples are considerably larger than those above comparable rough beds.

1. Introduction

The flow in the wave induced boundary layer at the sea bed influence many events of practical concern in the near-shore environment. These include the erosion or siltation of beaches, the attenuation of waves approaching the coast and the transport of pollutants. So, an improved understanding of the fluid phenomena behind these events is essential to enhance the present prediction capability and to provide solutions for the requirements and problems associated with the increasing use of the coastal zone for various activities, ranging from industrial to recreational, as well as for the growing public demand since late nineteen eighties for a cleaner, pleasant environment.

Manusctript received on : 10.06.2002
Manuscreipt accepted on : 05.02.2003

Most laboratory studies of wave boundary layer flow have been performed over flat beds, (e.g., detailed studies of Hino et al. 1983, Sleath 1987, Jensen 1989, Wijetunge and Sleath 1998, among many others). These results are therefore directly relevant to plane sea beds, despite the fact that the near-shore sea bottom is often covered with ripples. The limited number of experimental studies of wave motion over ripples include Horikawa and Watanabe, (1968), Du Toit and Sleath, (1981), Sato et al. (1987), Horikawa and Ikeda, (1990), Ranasoma and Sleath, (1992), Earnshaw et al. (1994), and Fredsoe et al. (1999). However, unfortunately, most of these studies are limited to a very narrow range of the relevant dimensionless parameters. Therefore, the primary objectives of the present paper are to examine the mean and turbulent flow quantities in wave boundary layer flow above ripples over a range of flow conditions and to provide more experimental data for the validation of models.

2. Experimental Set-up

The experiments were carried out in an oscillatory flow water tunnel, (see figure 1). This tunnel consists essentially of a U-tube in which water is caused to oscillate by a paddle driven by a variable speed motor. The rectangular working section of the tunnel is horizontal and 3.7 m long, 0.31 m wide and 0.45 m high.

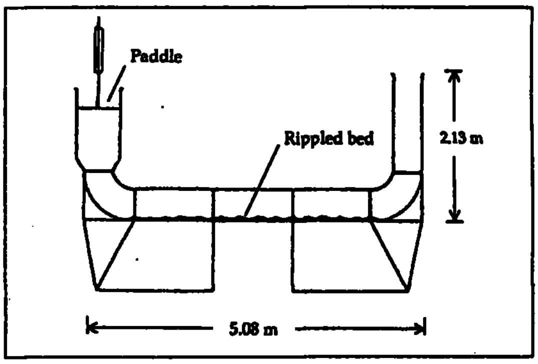

Figure 1: Oscillatory Flow Water Tunnel

Eng. (Dr.) Janaka J Wijethunga BSc Eng, PhD (Cambridge), AMIE(SL). Presently Senior Lecturer, Department of Civil Engineering, University of Peradeniya.

Under normal conditions the flow is almost sinusoidal, with the amplitude of the higher harmonics being less than 3% of the amplitude of the fundamental.

A rippled bed made out of hardwood was laid on the full length of the horizontal working section of the tunnel. The profile of the rippled bed used in the present study, (figure 2), is very similar to that of the ripples that form with 0.4 mm median diameter sand.

The fluid velocities, both the horizontal and the vertical components were measured simultaneously using a laser Doppler anemometer in forward scatter mode. These detailed measurements were made at ten vertical lines equally spaced over a ripple length. At each position, the velocity was sampled 100 times per cycle for 50 cycles. Both phase averaged (denoted by an overbar in the following) and root-mean-square velocities were then determined.

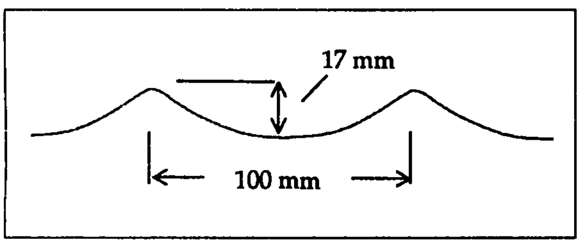

Figure 2: Profile of the Rippled Bed

3. Dimensional Analysis

It will help in the interpretation of the experimental results if we list the relevant dimensionless groups. We take the independent variables to be a, the orbital amplitude of the fluid just outside the boundary layer; h, the ripple height; L, the ripple wave length; t, time; T, the period of oscillation; x, the distance measured in the horizontal direction from the ripple crest; y, the distance measured in the vertical direction from the bed; and, the kinematic viscosity of the fluid.

Thus, any dependent variable may be expressed as a function of

$$\frac{a}{L}, \frac{\beta}{K}, \frac{h}{L}, \frac{x}{L}, ky, \omega t \quad (1)$$

where, $\omega = 2\pi/T$, $\beta = (\omega/2v)^{1/2}$, $k = 2\pi/L$.

Alternatively, if we treat ripples as roughness elements and assume that the roughness of the bottom boundary can be represented by an equivalent roughness length *ks* then the relevant dimensionless groups may be expressed as:

$$\frac{U_0 a}{v}, \frac{a}{k_s}, \frac{y}{k_s}, \omega t \quad (2)$$

In (2), U_0 is the amplitude of the free-stream velocity outside the boundary layer.

4. Test Conditions

The test conditions are summarized in Table 1. The range of a/L investigated in these tests was 0.12-3.35 and that of β/k was 12.4-20.8, whilst h/L was kept constant at 0.17. The values of a/L and h/L for ripples under field conditions mostly fall between 0.4-10 and 0.05-0.2, respectively, (Nielsen 1992).

Table 1: Test Conditions

Test No	U_0 m/s	T sec	V $x10^{-6}$ m2/s	a/L	β/k	$U_0 a/v$
1	0.016	4.58	1.12	0.12	12.4	171
2	0.058	4.71	1.08	0.44	12.5	2363
3	0.151	1.92	1.00	0.46	20.4	6946
4	0.081	4.83	1.02	0.62	12.7	4924
5	0.106	3.56	1.00	0.60	15.0	6360
6	0.197	1.93	0.97	0.60	20.6	12186
7	0.098	4.62	1.07	0.72	12.7	6594
8	0.112	4.49	1.09	0.80	12.8	8220
9	0.137	3.58	0.98	0.78	15.1	10904
10	0.265	1.92	0.96	0.81	20.8	22359
11	0.218	2.59	1.08	0.90	16.9	18167
12	0.222	4.61	1.01	1.63	13.1	35828
13	0.512	4.11	1.14	3.35	13.0	150456

5. Flow Regime

Figure 3 compares the present measurements with the criterion put forward by Sleath, (1975), for transition in oscillatory flow over rippled beds. We see that the flow conditions corresponding to test 1 are laminar, whereas all other tests lie above the lower limit for transition.

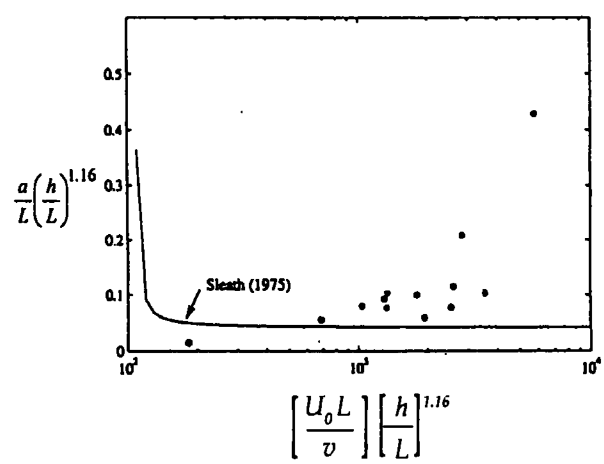

Figure 3: Flow regime: comparison of present measurements with the criterion of Sleath, (1975), for transition over ripples

Further, in the absence of a criterion for fully developed turbulence specifically obtained for rippled beds, we employ those obtained for flat rough beds, thus treating ripples as roughness elements. The roughness length of the bed *ks* was obtained using the formula suggested by Swart, (1976): $k_s = 25h^2/L$. Accordingly, the present measurements are compared with the criteria for fully developed turbulence suggested by Jonsson, (1966), and Sleath (1974) in figure 4. This suggests that the flow may be assumed turbulent for all tests except tests 1 and 2.

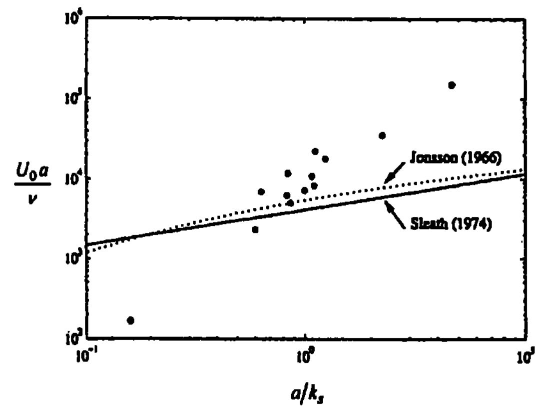

Figure 4: Flow regime: comparison of present measurements with criteria for fully developed turbulence over flat rough beds

6. Velocity Distribution over Ripples

6.1 Introduction

We first outline two theoretical solutions available for velocity distribution in wave boundary layer flow over ripples: one based on inviscid flow theory and the other is the classical laminar solution. This is followed by a comparison of the measured velocity profiles with the two theoretical solutions.

6.2 Theoretical Solutions

Inviscid flow solution

The physical z-plane above a rippled bed where the measurements were made, may be linked with the ζ-plane above a flat bed where the theoretical solution is obtained easily, using the transformation:

$$\zeta = z - i\frac{h}{2}e^{ik\zeta} \qquad (3)$$

where $z = x + iy$ and $\zeta = \xi + i\eta$. The assumed origin of the z-plane is $h/2$ below the ripple crest.

Thus the relation between the curvilinear coordinates (ξ, η) in the ζ-plane and the Cartesian coordinates (x,y) in the z-plane is obtained by expanding (3):

$$\zeta = x + \frac{h}{2} e^{-k\eta} \sin k\xi \qquad (4)$$

$$\eta = y - \frac{h}{2} e^{-k\eta} \cos k\xi \qquad (5)$$

The complex potential w in the upper half of the ζ plane is given by:

$$w = -U_0 \zeta \cos \omega t \qquad (6)$$

The corresponding velocity components (u_i, v_i) in the xy-plane are given by:

$$u_i - v_i = \frac{dw}{dz} = \frac{-U_0 \cos\omega t}{1 + \frac{hk}{2} e^{ik\zeta}} \qquad (7)$$

Expanding (7), we obtain

$$u_i = \frac{-U_0 \cos\omega t}{J}\left[1 - \frac{hk}{2} e^{-k\eta} \cos k\xi\right] \qquad (8)$$

$$v_i = \frac{U_0 \cos\omega t}{J}\left[\frac{hk}{2} e^{-k\eta} \sin k\xi\right] \qquad (9)$$

$$J = \left[1 - hke^{-k\eta} \cos k\xi + \left(\frac{hk}{2} e^{-k\eta}\right)^2\right] \qquad (10)$$

where J is the Jacobian of the transformation.

Laminar flow solution

Consider laminar flow in the oscillatory flow water tunnel above a smooth bed whose profile is given by (4 and 5). A first approximation for the horizontal component of velocity under these conditions is

$$u_l = -U_0 \left[\cos \omega t - e^{-\beta\eta} \cos(\omega t - \beta\eta)\right] \qquad (11)$$

provided that a and h are small compared with L (Sleath 1984).

6.3 Measured Velocity Profiles

Figure 5 shows the way in which the amplitude of the measured horizontal component of velocity above the crest and the trough varies with distance from the local bed level, y_l. The experimental data shown in this figure corresponds to Test 1. The very low values of the Reynolds number and a/L for this test means that there was no flow separation on the lee-side of the ripple crests. The dotted curves represent the corresponding inviscid flow solution, (8), whereas the solid curves show the laminar solution, (11). We see that the inviscid flow solution shows good agreement with the amplitude of the measured velocities except very close to the bed. The poor agreement close to the bed is not unexpected because viscous effects are significant in this very thin layer immediately adjacent to the bed. On the other hand, the laminar flow solution does not hold in the outer region, both above the crest and above the trough, though the agreement is better inside the thin viscous layer. This is not entirely surprising because, among other reasons, the present test conditions do not satisfy the requirement that $a, h << L$.

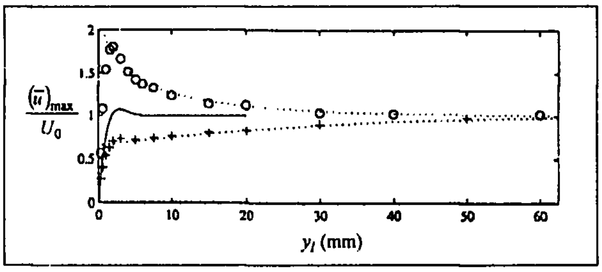

Figure 5: Variation with height above local bed level of amplitude of the horizontal component of velocity: crest traverse; + trough traverse, ... (8); ___ (11). Test 1

We now combine the inviscid and laminar flow solutions by replacing U_0 in (11) by the corresponding value given by (8). Consequently, the modified solution is obtained as

$$u_d = \frac{u_i u_l}{U_0 \cos \omega t} \qquad (12)$$

The measurements are compared with (12) in a separate figure , i.e., figure 6, to avoid confusion. The dashed curve shown in this figure is (12). Clearly, equation (12) shows good agreement with the amplitude of the measured velocities over the entire depth.

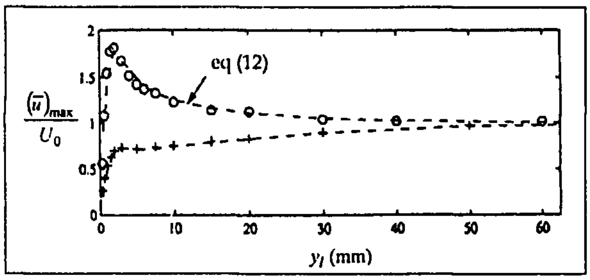

Figure 6: Comparison of measurements shown in figure 5 with (12): Test 1

However, if values of a/L were sufficiently large to cause flow separation at the ripple crest, one would not expect this inviscid flow solution to hold. This is because under such conditions near bed flow may be highly disturbed by the vortices that form on the lee-side of the ripples. Further, if the flow is turbulent, the increased effective viscosity may also modify the velocity distribution. Accordingly, we now examine the results from Test 7 in which both these phenomena may play a role.

Figure 7 shows the variation with height of the amplitude of the horizontal velocity above the crest and the trough. The dotted lines in these figures indicate the inviscid flow solution.

We see that the measured velocity amplitude profiles now deviate from the inviscid solution for $y_c < 50$, where y_c is the distance measured from the ripple crest level. This deviation appears to be particularly significant above the trough, except close to the bed. This is primarily due to the perturbations on the velocity amplitude arising from the dynamics of lee-vortices. Turbulence might have had an influence too.

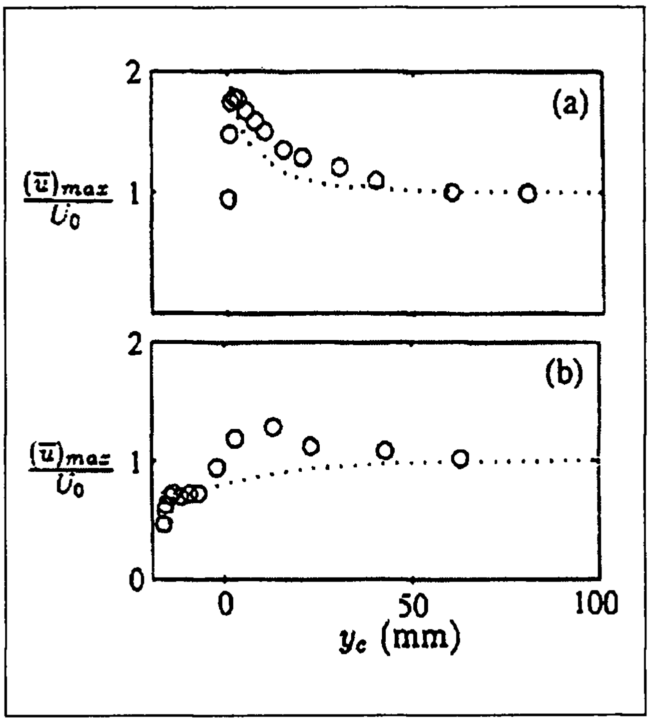

Figure 7: Variation with height of the amplitude of the horizontal velocity (a) above crest, (b) above trough. .... (8)

7. Vortex Dynamics

The velocity profiles discussed in Section 6 clearly indicate that the formation, growth and subsequent ejection of the lee-vortices have a considerable influence on the velocity distribution over ripples. Apparently, these vortices are also primarily responsible for sediment entrainment from ripple covered sea beds. Accordingly, here, we briefly examine the dynamics of the lee-vortices.

Figure 8 shows, in the form of velocity vectors, formation, growth and subsequent ejection of the lee-vortices over a half-cycle of oscillation. The corresponding vorticity contours are shown in figure 9.

Note that phase is measured relative to maximum negative velocity in the free-stream. We see that the lee-vortex experiences a rapid growth during the early stage of the decelerating part of the half cycle. Another notable feature is the surge in velocity over the lee-slope and the crest associated with the ejecting vortex, whilst free-stream velocity is nearly zero ($\omega t = 90^0$).

The vorticity plots also show that the vorticity of opposite sign generated along the bottom during the previous half cycle, further strengthened by the now ejecting vortex, seems to be responsible in triggering the next half cycle vortex. The ejected vortices travel close to the bed, confined mainly to $y_c / L < 0.4$. Further, at some instants, the travelling vortices are seen to split, with the leading part merging with the tail of the neighbouring vortex ($\omega t = 0^0 \rightarrow 40^0$ in figure 9).

8. Eulerian Drift Velocities

The time-mean velocity field near ripples is not zero due to the steady streaming set up by the wavy boundary. These steady drifts may be expected to play an important role in maintaining the equilibrium ripple profile.

The Eulerian drift velocities were obtained by taking the time-average of the velocity records. An example of the Eulerian velocity field over a ripple wave length is shown in figure 10. Clearly, there are two re-circulating cells per ripple wave length. It is also clear that the steady drifts are stronger near the bed on either side of the crest. The large velocities associated with the ejecting vortex is primarily responsible for the stronger drifts in the vicinity of the ripple crest. Since a net drift of fluid near the bed will also produce a net drift of sediment, these results shed some light on vortex ripple formation under wave motion.

Further, Figure 11 shows the way in which the peak values of the horizontal component of the drift velocities, u_r vary with a/L. As β/k for these tests is approximately constant, the curves show the effect of a/L on the peak drift velocities for a given value of h / L. Unfortunately, the initial parts of the curves are less clear due to lack of sufficient measurements in this region. Nevertheless, it appears that $(U_r)_{max} / U_0$ initially rises steeply with a / L, reaches a maximum and then falls again, over the range considered.

9. Comparison with Flat Rough Beds

9.1 Introduction

In the following, we briefly examine the applicability for turbulent wave boundary layer flow over ripples, of some of the established empirical or semi-empirical formulae that have been primarily derived for turbulent waves over flat rough beds. We use flow quantities averaged over a ripple wave length for the comparison. It must, however, be added that, in general, these relations have been obtained for larger values a / k_s of than those corresponding to the present investigation.

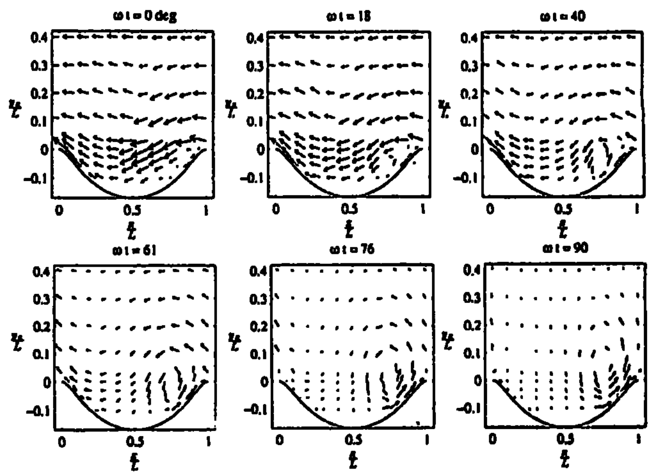

Figure 8: Velocity vectors: Test 2

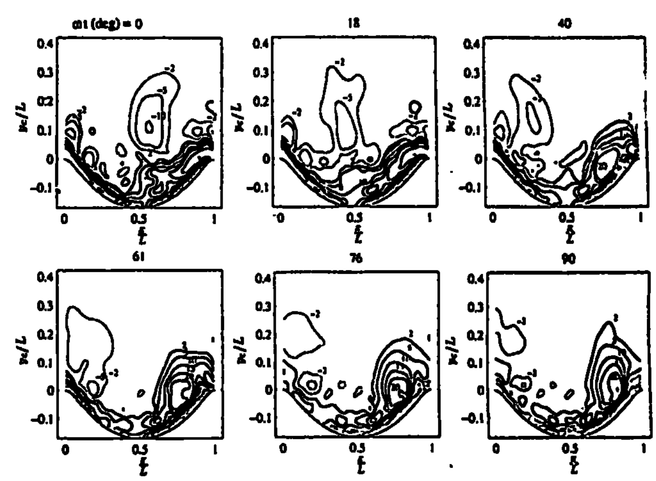

Figure 9: Vorticity contours: Test 2
clockwise circulation, counter- clockwise circulation

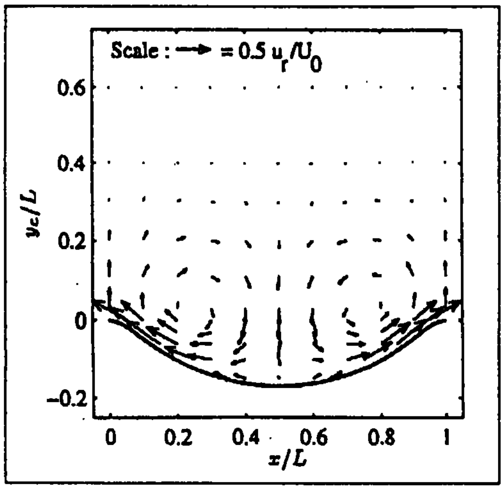

Figure 10: Eulerian drift velocity vectors: Test 5

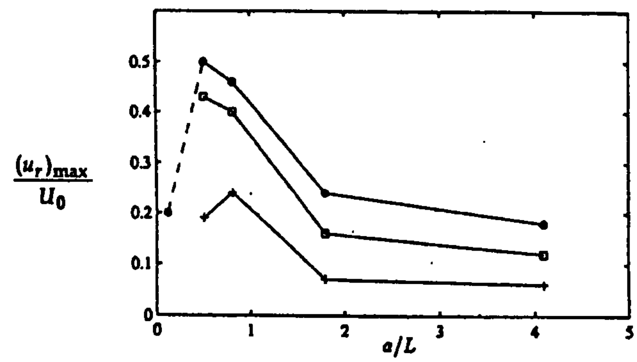

Figure 11: Variation with a/L of the peak values of the horizontal component of Eulerian drift velocities at different sections above the bed: x = L/8; L/4; + 3L/8.

9.2 Boundary Layer Thickness

Sleath, (1987), defined the wave boundary layer thickness as the distance measured from the bed out to the point at which the amplitude of the defect velocity, i.e., the difference between the free-stream velocity and the local velocity, is $0.05U_0$. This distance is denoted by σ. The experimental results for the thickness of the wave boundary layer over ripples, estimated from the definition of Sleath, are compared with results for flat rough beds in Figure 12.

The curve that fits the flat rough bed results of Sleath (1987) is:

$$\frac{\sigma}{k_s} = 0.27 \left(\frac{a}{k_s}\right)^{0.67} \qquad (13)$$

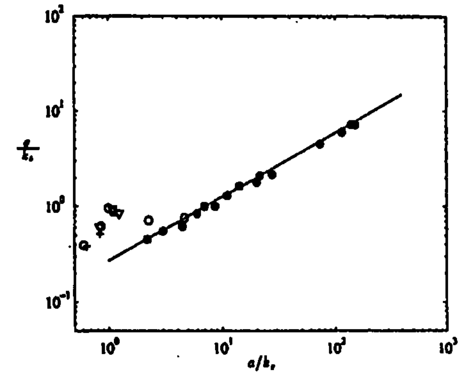

Figure 12: Thickness of boundary layer with a/ks: • Sleath (1987), Present measurements : $124 \le \beta / k \le 13.1$; ∇ $15.0 \le \beta / k \le 16.9$; + $20.4 \le \beta / k \le 20.8$; — (13)

We see in Figure 12 that the data points for ripples initially seem to deviate significantly away from the curve (13). Thereafter, the data points appear to approach (13) asymptotically with further increase in the parameter a/k_s.

9.3 Turbulence Intensities

The mean-square value of the turbulence component u' is given by:

$$\overline{u'^2}(x,y,t) = \frac{1}{N} \sum_{n=1}^{N} (u - \overline{u})^2 \qquad (14)$$

where, $\overline{u}$ is the phase-averaged velocity and N is the number of cycles of oscillation. The turbulence component v' was obtained using a similar expression.

Figure 13 compares the vertical and horizontal components of peak turbulence intensities over ripples with the measurements of Sleath, (1987), and Jensen (1989) above three-dimensional bed roughness such as beds of sand or gravel, over a range of the parameter a / k_s.

Clearly, the peak turbulence intensities over ripples are considerably higher than those over three-dimensional rough beds. However, we see that the present results for large a / k_s appear to approach those obtained for flat rough beds.

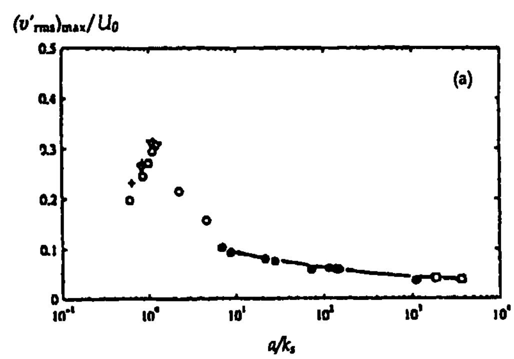

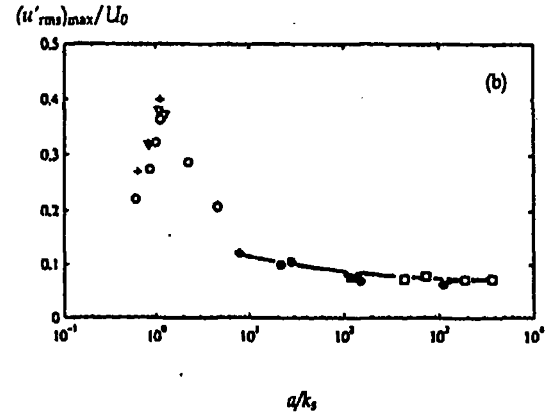

Figure 13: Comparison of the variation with a/k_s of the peak turbulence intensities, (a) vertical component, (b) horizontal component, over ripples with corresponding peak values above three dimensional bed roughness: •Sleath (1987); Jensen (1989); Present measurements; $12.4 \le \beta / k \le 13.1$; ∇ $15.0 \le \beta / k \le 16.9$; + $20.4 \le \beta / k \le 20.8$; — (13)

Further, the fact that the results for $15.0 \le \beta/k \le 16.9$ and $20.4 \le \beta/k \le 20.8$ lie along almost exactly the same curve suggests that this may represent the asymptotic curve (for high Reynolds numbers).In other words, the asymptotic curve starts to fall for values of a / k_s less than about 1. It was, however, not possible to carry out tests at values of $a / k_s > 1$ for a range of β / k and consequently we cannot be certain whether or not the curve obtained for $12.4 \le \beta / k \le 13.1$ is the asymptotic curve for $a /k_s > 1$. Moreover, whether this curve represents the fully developed turbulent conditions for ripples in general is not clear because we do not know how these quantities depend on the parameter h/L.

10. Conclusions

Detailed measurements of the velocities in wave boundary layer flow over a fixed bed of vortex ripples ($h/L = 0.17$) have been presented. The measurements were carried out over a range of the dimensionless parameters a /L (= 0.12 - 3.35) and β / k (= 12.4 - 20.8). For the range of conditions covered in these experiments the main conclusions are as follows:

1) Profiles of the amplitude of the measured horizontal component of velocity at $a / L = 0.12$ (Re = 171) showed good agreement with the potential flow solution except very close to the bed. The measurements, however, deviated considerably from the inviscid theory at relatively large values of , a / L mainly due to the perturbations from the lee-vortices.

(2) The dynamics of the vortices that form on the lee-side of the ripples has been examined using vorticity contours. The results show that the lee-vortices experience a rapid growth during the early stages of the formation. Further, the ejecting vortices induce a surge in velocity over the lee-slope and the crest, whilst the velocity in the free-stream is nearly zero. The ejected vortices travel close to the bed, confined mainly to $y_c / L < 0.4$.

(3) The Eulerian time-mean velocity field over ripples appears to consist of a single pair of recirculating cells. Further, the peak values of the horizontal component of the Eulerian drift velocities appear to rise steeply with a /L initially, reach a maximum and then fall again. The peak values for $a / L > 1$ are, in general, significantly smaller than those in the region $a / L > 1$.

(4) The thickness of the wave boundary layer over ripples appears to be larger than that over flat rough beds.

(5) Turbulence intensities over ripples are also considerably larger than those over comparable flat rough beds.

11. References

Du Toit, CG and Sleath, JFA (1981), Velocity measurements close to rippled beds in oscillatory flow, *J. Fluid Mech.*, 112, 71-96.

Earnshaw, HC, Bruce, T, Greated, CA and Easson, WJ (1994), PIV measurements of oscillatory flow over a rippled bed, Proc. 24th Conf. Coastal Eng., Kobe, 1975-1982.

Fredsoe, J., Andersen, KH and Sumer, M (1999), Wave plus current over a ripple covered bed, *Coastal Eng.*, 38, 177-221.

Hino, M, Kashiwayanagi, M, Nakayama, A and Hara, T (1976), Experiments on the turbulence statistics and the structure of a reciprocating oscillatory flow, *J. Fluid Mech.*, 131, 363-400.

Horikawa, K and Watanabe, A (1968), Laboratory study on oscillatory boundary layer flow, Proc. 12th Conf. Coastal Eng., Cape Town, 1335-1352.

Horikawa, K and Ikeda, S (1990), Characteristics of oscillatory flow over ripple models, Proc. 22nd Conf. Coastal Eng., Delft, 661-674.

Jensen, BL, Sumer, BM and Fredsoe, J (1989), Turbulent oscillatory boundary layers at high Reynolds numbers, *J. Fluid Mech.*, 206, 265-297.

Jonsson, IG (1966), Wave boundary layers and friction factors, Proc. 10th Conf. Coastal Eng., Tokyo, 127-148.

Nielsen, P (1992), *Coastal bottom boundary layers and sediment transport*, World Scientific, Singapore.

Ranasoma, KIM and Sleath, JFA (1992), Velocity measurements close to rippled beds, Proc. 22nd Conf. Coastal Eng., Venice, 2383-2396.

Sato, S, Shimosako, K and Watanabe, A (1987), Measurements of turbulent oscillatory boundary layer flow above ripples with a laser-doppler velocimeter, *Coastal Eng. In Japan*, **30**(1), 89-98.

Sleath, JFA (1974), Stability of laminar flow at sea bed, *ASCE J. Waterway, Port, Coastal and Ocean Eng. Div.*, **100** (WW2), 105 -122.

Sleath, JFA (1975), Transition in oscillatory flow over rippled beds, Proc. ICE, **59**, 309-322.

Sleath, JFA (1984), *Sea Bed Mechanics*, Wiley.

Sleath, JFA (1987), Turbulent oscillatory flow over rough beds, *J. Fluid Mech.*, **182**, 369-409.

Swart, DH (1976), Coastal sediment transport: computation of longshore transports, Delft Hydr. lab rep. R968(1).

Wijetunge, JJ and Sleath, JFA (1998), Effect of sediment transport on bed friction and turbulence, *ASCE J. Waterway, Port, Coastal and Ocean Eng. Div.*, **124** (4), 172-178.